Microtubule re-organization during female meiosis in *C. elegans*

Ina Lantzsch[1], Che-Hang Yu[2], Yu-Zen Chen[3,4], Vitaly Zimyanin[3,4], Hossein Yazdkhasti[3,4], Norbert Lindow[5], Erik Szentgyörgyi[1], Ariel Pani[6,7], Steffen Prohaska[5], Martin Srayko[8], Sebastian Fürthauer[9], and Stefanie Redemann[3,4,7]

[1] Experimental Center, Faculty of Medicine Carl Gustav Carus, Technische Universität Dresden, Germany
[2] Department of Electrical and Computer Engineering, University of California, Santa Barbara, CA, USA
[3] Center for Membrane and Cell Physiology, University of Virginia School of Medicine, Charlottesville, VA, USA.
[4] Department of Molecular Physiology and Biological Physics, University of Virginia, School of Medicine, Charlottesville, VA, USA
[5] Zuse Institute Berlin, 14195 Berlin, Germany
[6] Department of Biology, University of Virginia, Charlottesville, VA, USA
[7] Department of Cell Biology, University of Virginia School of Medicine, Charlottesville, VA, USA.
[8] Department of Biological Sciences, University of Alberta, Edmonton, Canada
[9] Center for Computational Biology, Flatiron Institute, NY, USA

Correspondence to: Stefanie Redemann (sz5j@virginia.edu), Sebastian Fürthauer (sfuerthauer@flatironinstitute.org)

Abstract

The female meiotic spindles of most animals are acentrosomal and undergo striking morphological changes while transitioning from metaphase to anaphase. The ultra-structure of acentrosomal spindles, and how changes to this structure correlate with such dramatic spindle rearrangements remains largely unknown.

To address this, we applied light microscopy, large-scale electron tomography and mathematical modeling of female meiotic *C. elegans* spindles undergoing the transition from metaphase to anaphase. Combining these approaches, we find that meiotic spindles are dynamic arrays of short microtubules that turn over on second time scales. The results show that the transition from metaphase to anaphase correlates with an increase in the number of microtubules and a decrease in their average length. Detailed analysis of the tomographic data revealed that the length of microtubules changes significantly during

the metaphase-to-anaphase transition. This effect is most pronounced for those microtubules located within 150 nm of the chromosome surface. To understand the mechanisms that drive this transition, we developed a mathematical model for the microtubule length distribution that considers microtubule growth, catastrophe, and severing. Using Bayesian inference to compare model predictions and data, we find that microtubule turn-over is the major driver of the observed large-scale reorganizations. Our data suggest that in metaphase only a minor fraction of microtubules, those that are closest to the chromosomes, are severed. The large majority of microtubules, which are not in close contact with chromosomes, do not undergo severing. Instead, their length distribution is fully explained by growth and catastrophe alone. In anaphase, even microtubules close to the chromosomes show no signs of cutting. This suggests that the most prominent drivers of spindle rearrangements from metaphase to anaphase are changes in nucleation and catastrophe rate. In addition, we provide evidence that microtubule severing is dependent on the presence of katanin.

Introduction

During meiosis, haploid gametes are produced from diploid progenitor cells in most sexually reproducing eukaryotes. The reduction of chromosome number in the gametes is essential for the development of the fertilized oocyte into an embryo. Therefore, the accuracy of meiosis is crucial, as errors in chromosome segregation result in aneuploidies and lead to genetic disorders, which are often lethal (Hassold & Hunt 2001).

In this paper, we study the structure and dynamics of female meiotic spindles in *C. elegans*. Female meiotic spindles, like mitotic and male meiotic spindles, are built from microtubules (MTs), motor proteins and microtubule-associated proteins. However, unlike other spindles in most animals, female meiotic spindles typically have no centrosomes, due to centriole elimination during oogenesis. Thus, female meiotic spindles are assembled differently from those that rely on centrosome-based microtubule-

organizing centers. Specifically, this is true in humans (Holubcová et al., 2015), mice (Schuh and Ellenberg, 2007) and also in nematodes (Albertson and Thomson, 1993). It is an open question how their structure reflects the differences in assembly.

In *C. elegans*, female meiotic spindles undergo a drastic reorganization during the metaphase-to-anaphase transition. During metaphase of meiosis I and II, microtubules form a pointed and elongated bipolar spindle, which then shortens during anaphase. In addition, the microtubule density shifts from the spindle poles to the midzone between the separating chromosomes. This mid-zone then extends until the end of anaphase (Dumont et al., 2010; Laband et al., 2017, Yu et al 2019). The structural basis of these rearrangements and their role in meiotic chromosome segregation are not well understood. In particular, it remains unclear whether these structural rearrangements are driven by katanin-mediated severing (Joly et al 2016, Srayko et al 2006), transport (Mullen & Wignall 2017, Brugués et al 2012) or changes in MT nucleation or polymerization dynamics (Brugués et al 2012, Needleman et al 2010).

Here, we study the mechanisms of structural microtubule arrangement by using large-scale electron tomography (Redemann et al 2017 & 2018, Fabig et al 2020) to obtain the 3D ultrastructure of spindles in *C. elegans* oocyte meiosis. We find that female meiotic spindles are composed of arrays of short microtubules, 90% are shorter than half spindle length, which are highly dynamic and turn-over within 10 seconds. During the transition from metaphase to anaphase, the number and lengths of microtubules change significantly. To understand the drivers of these changes we developed a mathematical model for the length distributions of microtubules that includes life time (turn-over), growth, and microtubule severing. We inferred the parameters of the model from data using Bayesian inference and Markov Chain Monte Carlo sampling. Our data suggest that the changes in microtubule number and lengths are mostly caused by changing microtubule turnover. While severing clearly occurs during metaphase, our data suggests that it affects only the small fraction of microtubules which contact the chromosomes. Here and in the following, we define that a microtubule contacts a chromosome if any point of its lattice is within

150nm of a chromosomes surface. The rearrangements of spindle architecture towards anaphase are likely caused by changes in nucleation and not by any changes in cutting rates.

Results

Three-dimensional reconstruction reveals structural changes of the spindle throughout female meiosis

Previous analyses of meiotic spindle microtubules using EM tomography were based on partial, rather than full, reconstructions of the spindle. This made it impossible to measure the total length of microtubules composing the spindle, since most microtubules extend beyond the tomographic volume.

We obtained the spindle ultrastructure of *C. elegans* oocytes by serial-section electron tomography, which allows the reconstruction of whole spindles in 3D with single-microtubule resolution (Redemann et al., 2017 & 2018). We reconstructed two meiotic spindles in metaphase I (T0243.5 and T0243.7), as well as four spindles at early (T0243.4), mid (T0208.1) and late stages of anaphase I (T0275.10 and T0369.8; Fig. 1A, Suppl. Movie 1-3) for meiosis I. In addition, we reconstructed two metaphases (T0186.1 and T0209.7), one early anaphase (T0186.3), and one mid anaphase (T0234.6) stage of meiosis II oocytes (Fig. 1B). We had previously analyzed the modes of microtubule attachment to chromosomes (end-on *vs.* lateral) and discussed the resulting role of microtubules in chromosome segregation during anaphase using the Meiosis I metaphase (T0243.5), early anaphase (T0243.4), mid anaphase datasets (T0208.1) (Redemann et al 2018) and late anaphase (T0275.10) (Yu et al 2019) of the first meiotic division. Here, we used those datasets, together with newly generated additional datasets of meiosis I metaphase (T0243.7), and late anaphase (T0369.8), and two meiosis II metaphases (T0186.1, T0209.7), early anaphase (T0186.3) and mid anaphase (T0234.6) to quantitatively characterize the spindle structure and microtubule rearrangements during female meiosis.

For this, we compiled summary statistics that characterize spindle morphology. In Table 1 we report the spindle length, the number of microtubules, the number of microtubules that are located within 150 nm

from the chromosome surface, the average microtubule length, the maximum microtubule length, the total polymer length (added length of all microtubules), the dimension of the tomogram and spindle dimensions for each stage of meiosis I and II (Table 1). We also indicated new and previously analyzed datasets in this table.

Meiosis I	MI Metaphase T0243.5	MI Metaphase T0243.7 *	MI early Ana T0243.4	MI mid Ana T0208.1	MI late Ana T0275.10 *	MI late Ana T0369.8 *
Spindle length	5 μm	5.4 μm	3.1 μm	2.7 μm	4.5 μm	5.1 μm
Number of MTs	3662	3812	7011	3317	1511	1306
MT within 150nm	500	920	5361	2334	875	699
Average MT length	0.91 ± 0.08 μm	1.04 ± 0.93 μm	0.58 ± 0.52 μm	0.62 ± 0.49 μm	0.74 ± 0.54 μm	0.55 ± 0.45μm
Max. MT length	5 μm	5.4 μm	5 μm	3.2 μm	4.2 μm	2.9 μm
Net polymer length	3338 μm	3961μm	4045 μm	2061 μm	1111 μm	724 μm
Tomogram dimension	9.1 x 9.7 x 3.8 μm	9.1 x 8 x 2.1 μm	5 x 5.9 x 2.8 μm	5.5 x 6.6 x 4.1 μm	7.5 x 5.6 x 2.6 μm	6.9 x 5.5 x 2.6 μm
Spindle dimension	5 x 8 x 3.9 μm	5.4 x 5.6 x 2.1 μm	3.1 x 4.3 x 2.6 μm	2.7 x 3 x 2.5 μm	4.5 x 1.2 x 1 μm	5.1 x 1.4 x 0.8 μm

Meiosis II	MII Metaphase T0186.1 *	MII Metaphase T0209.7 *	MII early Ana T0186.3 *	MII mid Ana T0234.6 *
Spindle length	5.9 μm	5.8 μm	4.0 μm	2.5 μm
Number of MTs	3013	3808	5572	2246
MT within 150nm	484	887	3298	1359
Average MT length	0.68 ± 0.76 μm	1.11 ± 0.92 μm	0.90 ± 0.79 μm	0.57 ± 0.491 μm
Max. MT length	4.7 μm	5.8 μm	4.8 μm	2.8 μm
Net polymer length	2693 μm	4237 μm	4512 μm	1236 μm
Tomogram dimension	8.6 x 9.8 x 3.3 μm	11 x 5.5 x 2.8 μm	5.6 x 6.9 x 2.7 μm	9 x 6.2 x 3.3 μm
Spindle dimension	5.9 x 5.8 x 3.8 μm	5.8 x 4.1 x 3.1 μm	4 x 4.1 x 3.3 μm	2.5 x 3.7 x 2.8 μm

Table 1. Summary of quantifications of tomographic data for meiosis I and meiosis II

*The spindle length, the total number of microtubules, the number of microtubules within 150 nm from the chromosome surface, the average microtubule length, the maximum length of microtubules, the total length of all microtubules (net polymer length) in the spindle, the dimension of the tomogram and spindle dimensions are shown for each tomographic data set. The * labels newly generated datasets.*

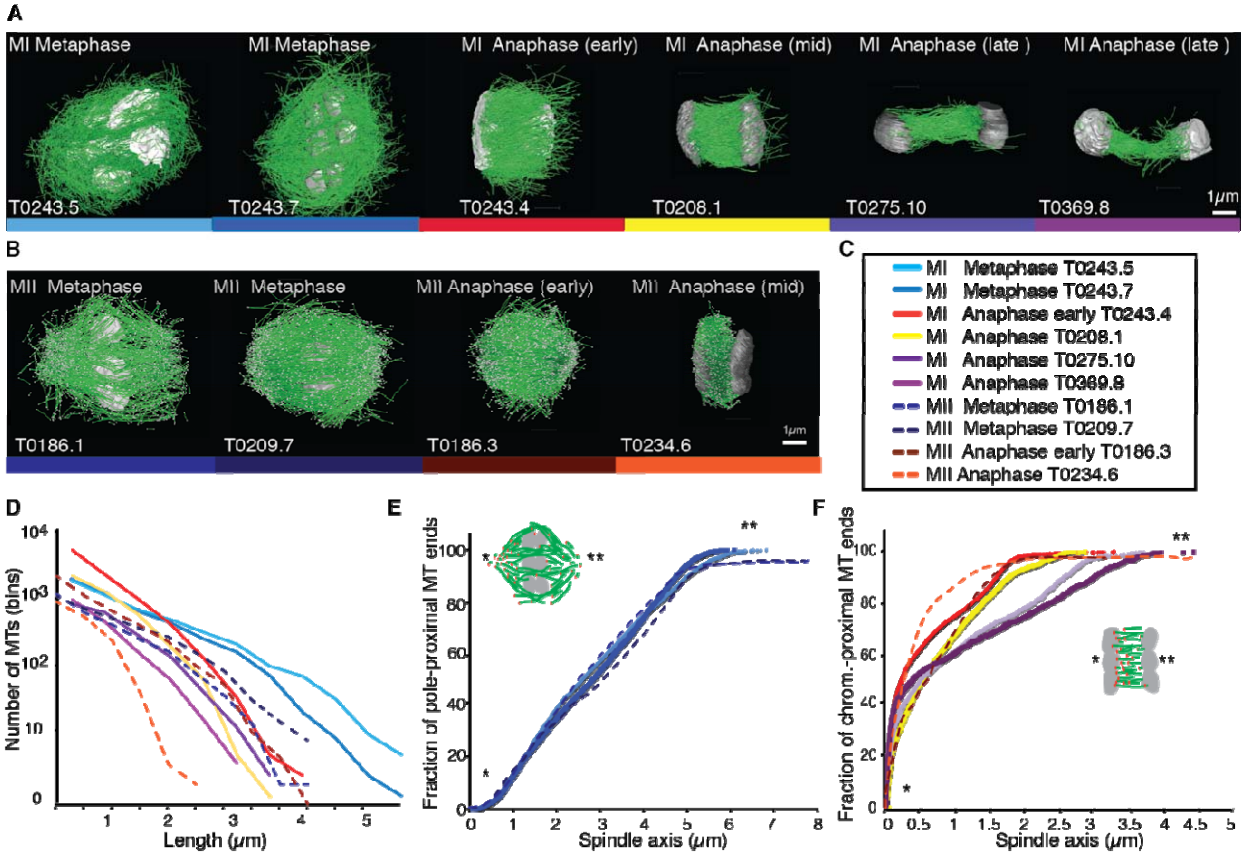

Figure 1

Figure 1. Three-dimensional organization of microtubules in meiosis I and II

A*, Three-dimensional models showing full reconstruction of microtubules at different stages of wild-type meiosis I. The different stages from metaphase to late anaphase are indicated. Microtubules are shown in green, chromosomes in grey. An individual color is assigned to each data set. The anaphase datasets are oriented with the cortical side being left, cytoplasmic right.* ***B****, Like* ***A*** *but three-dimensional models showing full reconstruction of microtubules at different stages of wild-type meiosis II.* ***C****, Legend for the different datasets plotted in Figures* ***D-F****.* ***D****, Length distribution of microtubules composing the different spindles. Bin size 250nm* ***E****, Cumulative distance function of the pole-proximal microtubule endpoints in metaphase of meiosis I and II. The position of the spindle poles in the schematic drawing and the data sets is indicated (stars).* ***F****, Cumulative distance function of the chromosome-proximal microtubule endpoints in anaphase. The position of the poles is indicated (stars).*

Female meiotic spindles are arrays of short microtubules

We first sought to characterize the overall spindle structure. Female meiotic spindles could be constructed mainly from long microtubules, reaching from near the spindle pole to chromosomes (as in *C. elegans* mitotic spindles; Redemann et al 2017), or from short ones distributed throughout the spindle volume, as

suggested by Srayko et al., 2006, and for instance, meiotic *Xenopus* spindles (Brugués et al 2012, Burbank et al 2006, Yang et al 2007).

Our data show that throughout meiosis I and meiosis II, roughly 40-50% of microtubules are shorter than 500 nm (Fig. 1D). In contrast, the fraction of microtubules that are at least half spindle length or longer is only 10%. Throughout meiosis the mean length of microtubules is approximately 20% of the spindle length

(Table 1). Furthermore, we determined the position of the pole-proximal ends of microtubules along the spindle axis. In metaphase, these putative microtubule minus-ends were found throughout the spindle (Fig. 1E), with no marked preference for the poles. In anaphase, about 60-70% of microtubules are found within a distance of 150 nm from the chromosomes, and the others are distributed throughout the spindle (Fig. 1F).

Together, these findings directly confirm, that the acentrosomal female meiotic *C. elegans* spindle is an array of short microtubules, more similar to meiotic Xenopus spindles than to mitotic spindles in *C. elegans*, as previously inferred by others based on light microscopy (Brugués et al 2012, Burbank et al 2006, Yang et al 2007). We conclude that the distance between poles in metaphase (5 µm) and chromosomes in anaphase (3-4 µm) is bridged by an array of short overlapping microtubules rather than long ones spanning the entire distance. This is an overall interesting finding, as *C. elegans* meiotic spindles are rather short in comparison to Xenopus meiotic spindles, and could easily generate microtubules long enough to bridge the entire spindle length, which is much harder to achieve in a 60 µm Xenopus spindle.

Meiotic spindles are composed of short-lived, fast moving microtubules

We next sought to understand the role of microtubule movements and dynamics in the structural changes observed during the transition from metaphase to anaphase. Since electron tomography generates static

snapshots, we investigated this question by light microscopy. Using Fluorescence Recovery After Photobleaching (FRAP), we first measured microtubule turnover and motion in metaphase I spindles. By photobleaching a small stripe near the center as well as close to the

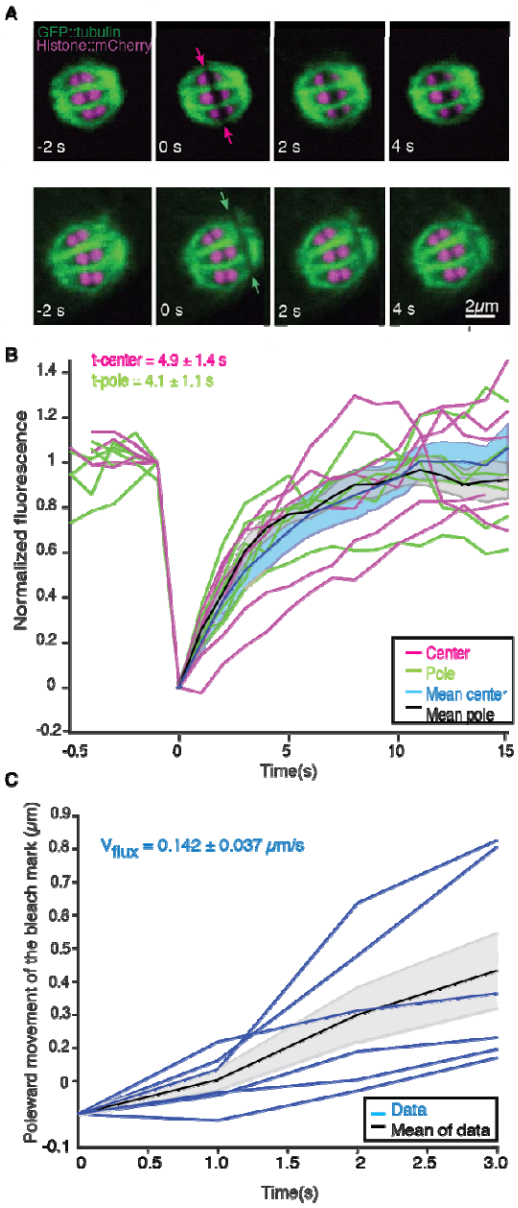

Figure 2

Figure 2. Microtubule dynamics during metaphase of meiosis I

A*, Light microscope images of spindles in meiosis I prior to and after photo bleaching at the spindle center (top row, red arrows) and close to the spindle pole (bottom row, green arrows). The bleaching of the sample (t=0) and the frame rate are indicated.* ***B****, Plot of the recovery of the bleach mark over time at the center (magenta, mean values given in blue) and pole (green, mean values given in black) for different datasets. The recovery times for the data sets are shown in the plot.* ***C****, Plot showing the poleward motion of the bleach mark at the spindle pole over time for different datasets (blue). The mean is indicated in black.*

poles of metaphase spindles (Fig. 2A, arrows, Suppl. Movie 4), we observed a half-time of microtubule recovery in metaphase of 4.9 s ± 3.4 s (n=6) in the spindle center and 4.1 s ± 2.7 s (n=6) at the spindle poles (Fig. 2B). In addition, we observed that the photo-bleached stripes close to the spindle poles showed a rapid poleward movement with a rate of 8.5 ± 2.2 µm/min (n=6, Fig.2C).

We conclude that microtubules in *C. elegans* meiosis turn over rapidly and show substantial poleward motion. This is notably different from the first mitotic division in the early *C. elegans* embryos, where microtubule motion was not detected in similar experiments (Labbe et al., 2004; Redemann et al., 2017). Thus, in female meiosis, both nucleation/depolymerization and microtubule motion might be involved in shaping the spindle structure. Similar microtubule dynamics have been described in Xenopus meiotic spindles using fluorescent speckle microscopy (Burbank et al 2006, Yang et al 2007 Burbank et al 2006, Yang et al 2007).

Spindle rearrangements during meiosis correlate with substantial changes in microtubule number.

To better understand the role of microtubule polymerization dynamics, we next asked whether the number of spindle microtubules changed during spindle rearrangements. From our reconstructions we detected 3662 and 3812 microtubules in metaphase of meiosis I (3013 and 3808 in meiosis II), 7011 microtubules in early anaphase of meiosis I (5572 in meiosis II) 3317 in mid anaphase of meiosis I (2246 in meiosis II) and 1511 and 1306 microtubules in late anaphase of meiosis I (Table 1). This shows that the number of microtubules almost doubles between metaphase and early anaphase. To get a more spatially resolved picture, we also measured the number of microtubules along the spindle axis in our datasets. This measurement showed that the number of microtubules increases by more than 2-fold in the center of the spindle from metaphase to early anaphase, while the number of microtubules at the spindle poles only slightly increases from metaphase to early anaphase and then decreases throughout anaphase (Fig. 3A). During anaphase, the number of microtubules decreased on the poles and almost halved in the spindle center (Fig. 3A,B). Thus, we conclude that changing the number of microtubules is correlated with the structural spindle rearrangements that occur during meiosis.

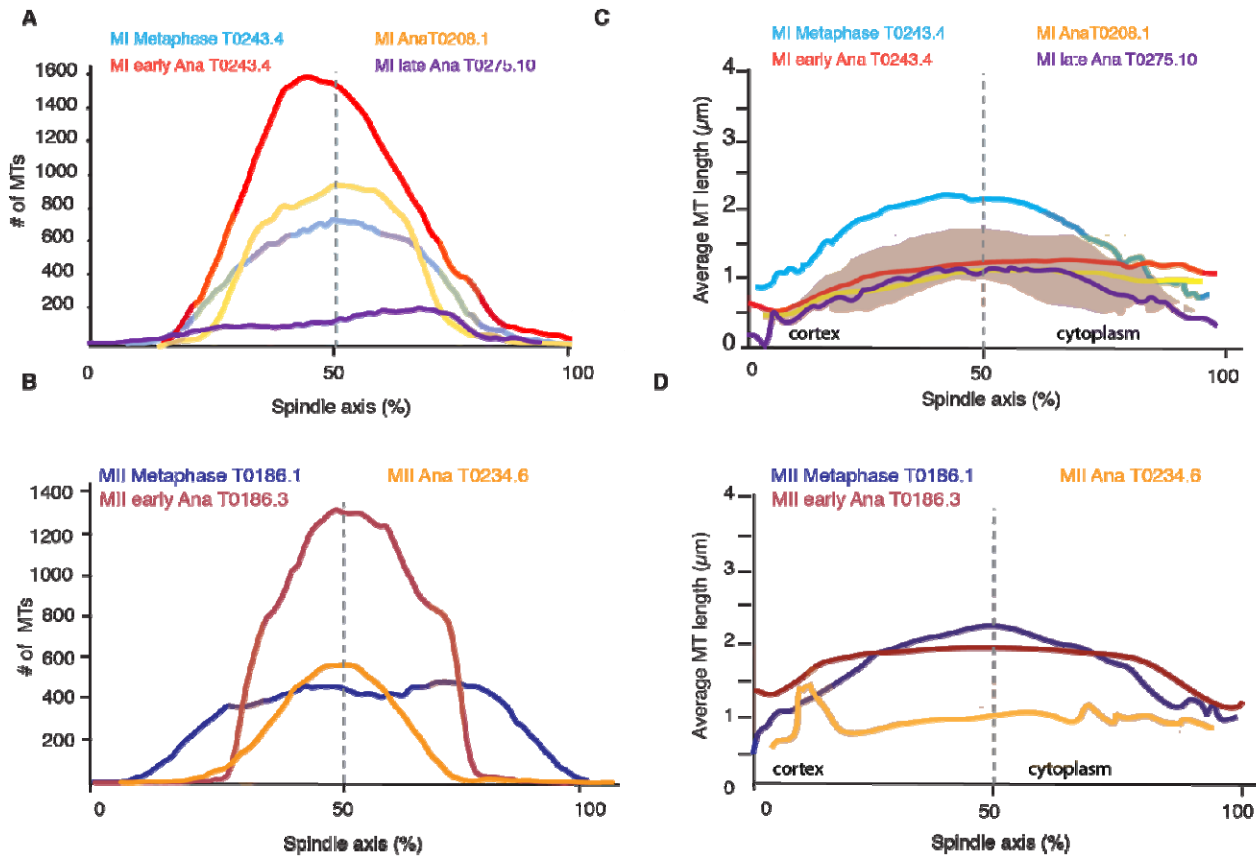

Figure 3

Figure 3. Analysis of microtubule number and length along the spindle axis

A*, Plot of the number of microtubules at different positions (100 nm steps) along the spindle axis for four different datasets in metaphase, early anaphase, mid and late anaphase in meiosis I. The approximate position of chromosomes for each dataset is indicated by the colored ovals. The datasets are oriented with '0' being at the cortical side. Datasets are aligned with the center of the spindle located at 50%* ***B****, Same plot as in* ***A*** *but for meiosis II.* ***C****, Plot of the average microtubule length at different positions (100nm steps) along the spindle axis for four different datasets in metaphase, early anaphase, mid and late anaphase. Shaded color indicates the standard deviation, datasets are oriented with '0' being at the cortical side. Datasets are aligned with the center of the spindle located at 50%* ***D,*** *Same plot as in* ***C*** *but for meiosis II*

Microtubule rearrangements during meiosis are driven by changes in microtubule dynamics, not nucleation rates alone.

We next sought to gain insight into the mechanisms that drive the observed changes in microtubule numbers. We first asked whether changes in nucleation rate alone could explain the data. If this were the

case, microtubule growth, shrinkage, and severing rates would remain the same, and the average length of the microtubules would remain unchanged throughout meiosis. However, the total polymer amount, the length of all microtubules added together, would change in step with the microtubule number.

Interestingly, we found the opposite result: the total polymer length of microtubules remained almost constant from metaphase to anaphase even though the number of microtubules increases 2-fold (Table 1). Furthermore, during the same time, the average length of microtubules went down by a factor of 2 (Fig. 1D, Table 1). Only in late anaphase, as the spindle continued to elongate, did the number of microtubules and the total polymer length start to decrease. Therefore, the observed changes in spindle morphology were not caused by changes in nucleation rates alone, but also by changes in microtubule disassembly. In principle this could be caused by local or global changes in microtubule severing, changes in microtubule growth dynamics, or a combination thereof. In the following, we will try to disentangle these possibilities.

Microtubule dynamics during spindle rearrangement are globally regulated

We next investigated whether changes in microtubule length were uniform along the spindle axis by quantifying the average microtubule length along the spindle axis. This analysis revealed that, during the transition from metaphase to early anaphase, the average length of microtubules decreased everywhere in the spindle (Fig.3 C, D). However, the magnitude of the decrease in length varies as a function of position. The average length of microtubules in the middle of the spindle decreased nearly twice as much as the average length of microtubules near the spindle poles (Fig. 3 C, D,). The analysis of average microtubule length along the axis also showed that in all spindles, in metaphase and in anaphase, the average length of microtubules is shorter near the spindle poles (Fig. 3C, D), which in anaphase is located at the inner surface of the chromosomes.

We more closely mapped the position of microtubules according to their length (Fig. 4A-G) by plotting the number of microtubules that are 500 nm and shorter as well as the number of microtubules between 0.5-1 µm and 1-1.5 µm along the spindle axis (Fig. 4H-N). This analysis showed that short microtubules,

500 nm and below, are localized closer to the spindle poles, while longer microtubules, between 0.51-

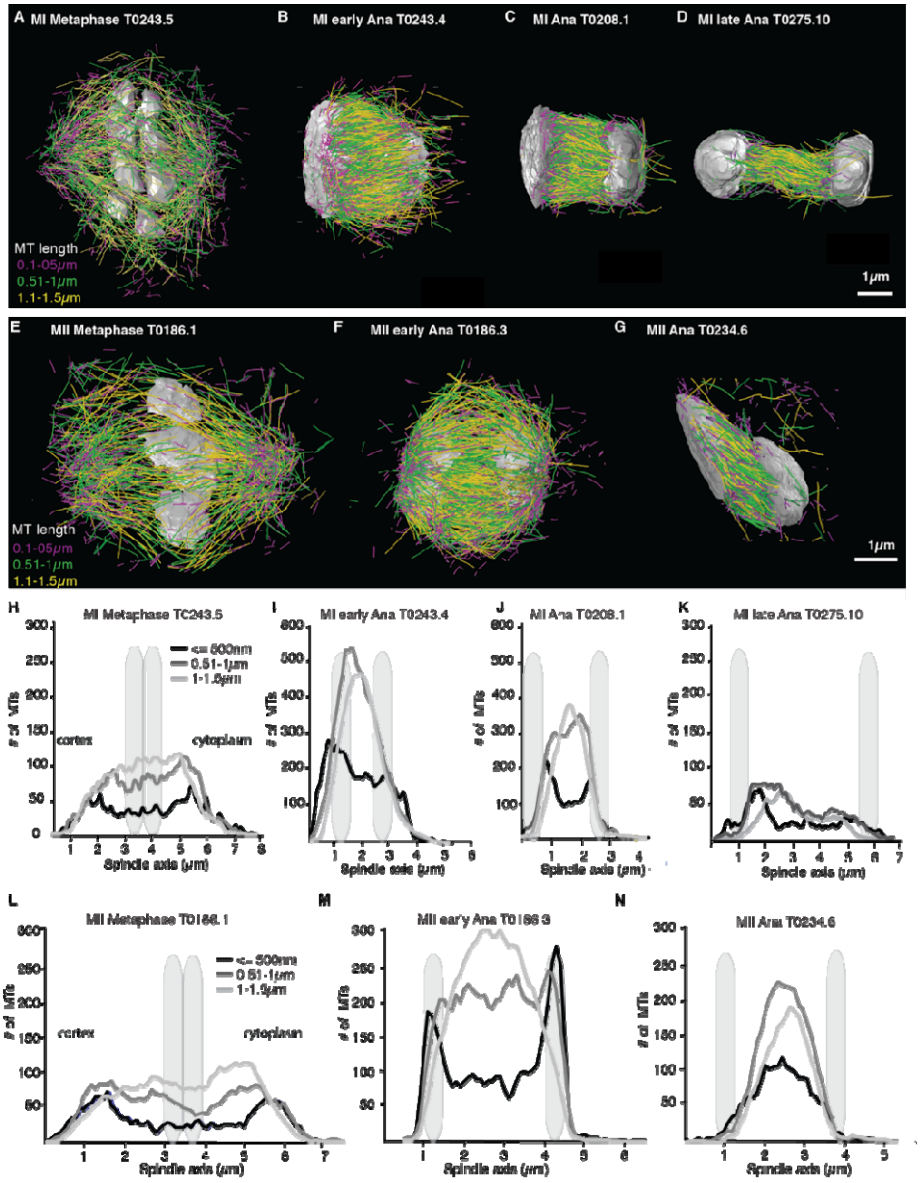

1.5µm, are **Figure 4**

Figure 4. Analysis of microtubule number according to their length along the spindle axis

A-G*, Tomographic reconstructions of meiotic spindles in meiosis I and II showing microtubules of different length. Microtubules with length =< 500nm are magenta, microtubules between 0.51-1µm are green and microtubules between 1.1-1.5µm are yellow. Chromosomes are grey, spindles are oriented with the cortical site to the left. Scale bar 1µm.* ***H-N****, Plots showing the number of microtubules according to their length along the spindle axis for the datasets shown in* ***A-G****. Dark line shows the number of microtubules <= 500nm, medium grey line microtubules between 0.5-1µm and light grey lines microtubules between 1-1.5µm. The approximate position of chromosomes is indicated by grey outlines.*

localized to the spindle center. We also found that the number of short microtubules increased from approximately 35% of all microtubules in metaphase to 50% of all microtubules in anaphase (Fig. 4 A-G). Throughout anaphase, we noticed that there were more short microtubules in the spindle half closer to the cell cortex (Fig. 3,4). This difference was most apparent in early and mid anaphase, where the average microtubule length in the cortical spindle half was 1.00 µm ± 0.6 (p = 3.6 E-6) and 1.17 µm ± 0.8 in the cytoplasmic half, and in early anaphase with an average length of 0.91 ± 0.53 (p = 0.002) in the cortical half and 1.04 µm ± 0.6 in the cytoplasmic half. We do not know at this point what causes this asymmetry.

Together, our data suggest that microtubule dynamics change throughout the spindle during spindle rearrangements. While the magnitude of this effect is spatially varying, throughout the spindle nucleation and turnover rates increase.

Bayesian inference on a mathematical model for microtubule dynamics reveals the relative importance of microtubule severing and growth dynamics for the global spindle dynamics

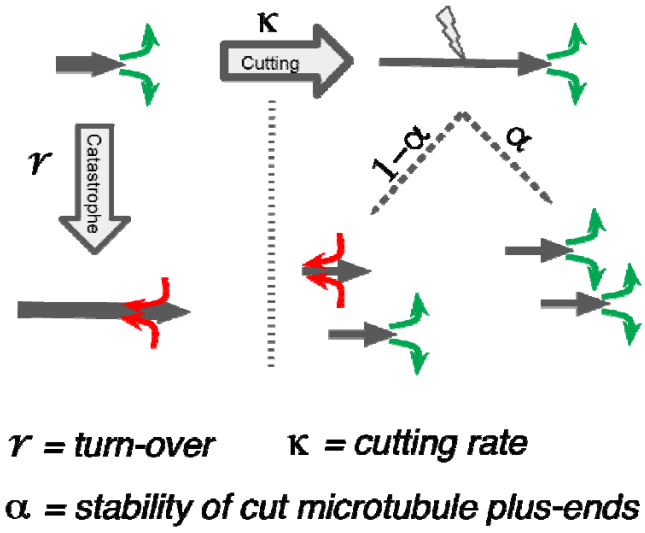

Figure 5

We next sought to better understand the processes that drive the observed microtubule length changes during spindle rearrangements. For this we constructed a mathematical model that solves for the expected microtubule length distribution given their growth velocity v_g, their rate of undergoing catastrophe r and the rate at which microtubules are cut per unit time and length κ. The stability of microtubule plus ends created by

Figure 5. Processes determining microtubule length Distributions

Our model considers microtubule turnover with a rate r, and cutting with a rate kappa. Alpha is the stability of cutting generated MT plus-ends.

cutting, is encoded in the parameter α, which interpolates between the two extreme cases, where newly created plus ends immediately depolymerize (α = 0) and where newly created plus ends are indistinguishable from preexisting ones (α = 1; see Fig. 5). The mathematical details of this model are given in the appendix (Suppl. Material 1). In spirit, it is very similar to the model proposed in (Kuo et al 2019).

We used this mathematical model to infer the relative importance of microtubule cutting and changes in microtubule nucleation. Using Markov Chain Monte Carlo sampling (Foreman-Mackey et al 2013, MacKay & MacKay 2003), we infer the most likely values for the dimensionless ratios $\bar{r} = r/v_g\ell$ and $\bar{\kappa} = \kappa/v_g\ell^2$predict the location of the average microtubule lengths ℓ, given the experimentally determined microtubule length distribution (see Appendix 1). Importantly this inference scheme only uses the experimentally measured microtubule length distribution as input, and allows us to quantify the relative importance of cutting to turnover $\bar{r}/\bar{\kappa}$ independently of direct measurements of turnover rates and microtubule growth velocities, which are hard to do in these very small spindles. We note that additional experiments like FRAP allow us to give absolute time units, since it directly measures the turnover rate. The results of the inference scheme are however independent of the FRAP measurements. For details, we refer the reader to the supplementary material Appendix 1.

Using this approach, we first sought to infer the relative importance of turnover to cutting throughout the spindle. In Figure 6 we show the inferred posterior probabilities of model parameters based on the data (Fig. 6A-D, Suppl. Fig. 1 A-D). These plots give the most likely values of the model parameters given the data, 95% confidence intervals for each of the parameters and 2D error plots for each pair of parameters under the assumption that the third is at its most likely value. We also compared the predictions of the

model parameterized by the expectation values of all parameters to our data (Fig. 6E-H, Suppl. Fig.1 E-H).

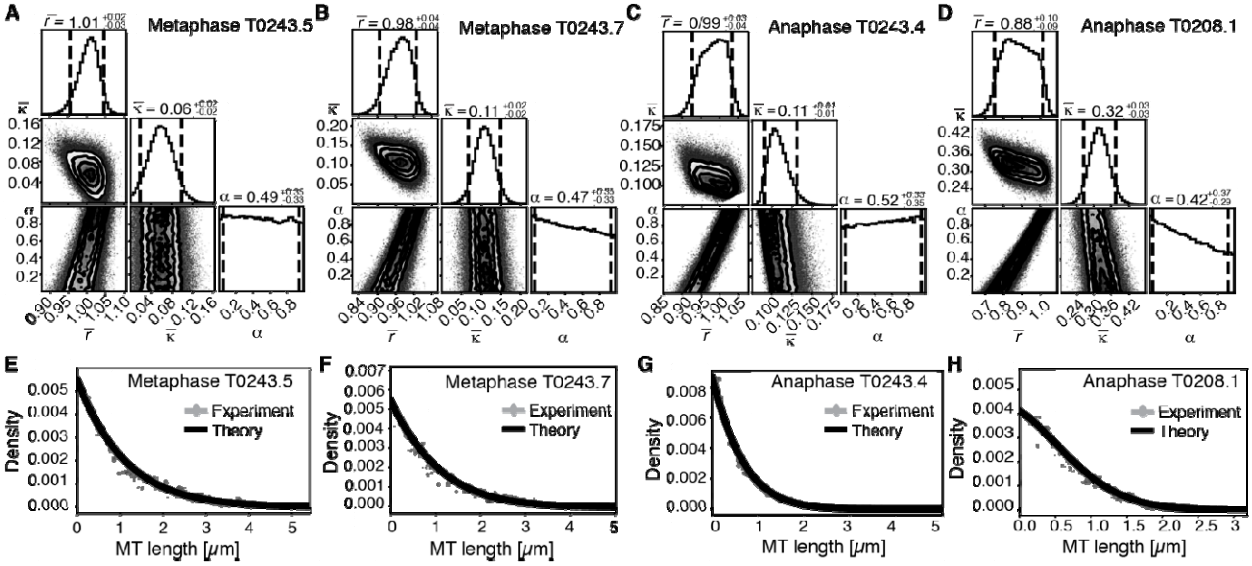

Figure 6

Figure 6. Inference of model parameters in metaphase and anaphase spindles

A*, Likelihood distribution of model parameters determined by Markov Chain Monte-Carlo for Metaphase T0243.5. The top boxes show the totally marginalized distribution of parameters, with dashed lines delimiting the 95% confidence interval. Surface plots show cuts through the likelihood distributions, marginalized onto 2D subspaces. Lines are contour lines, dots indicate MCMC-samples.* ***B****, Same as in* ***A*** *but for the Metaphase T0243.7 dataset.* ***C****, Same as in* ***A*** *but for the early Anaphase T0243.4 dataset.* ***D****, Same as in* ***A*** *but for the mid Anaphase T0208.1 dataset.* ***E, F, G, H*** *Comparison of experimentally determined length distribution of microtubules (dots) to the prediction of the highest likelihood model (solid line) for Metaphase T0243.5 (****E****), Metaphase T0243.7 (****F****), early Anaphase T0243.4 (****G****) and mid Anaphase T0208.1 (****H****). Plots for meiosis II can be found in Supplementary Figure 1.*

We asked whether the transition of spindle structure from metaphase to early anaphase can be explained by microtubule turnover, which here means changes in growth rate and catastrophe, or microtubule cutting. We report our results in terms of the non-dimensionalized turnover rate $\bar{r} = r/v_g\ell$, and the non-dimensionalized cutting rate $\bar{\kappa} = \kappa/v_g\ell^2$ where ℓ is the average microtubule length. Most importantly the ratio of these two quantities $\bar{r}/\bar{\kappa}$ gives the length (in units of average MT length) a microtubule has to reach for it to be more likely to get severed than to undergo catastrophe. This quantifies the relative importance of turnover to cutting; for example, if $\bar{r}/\bar{\kappa}$ it is much smaller than 1, then this indicates a

length distribution that is dominated by cutting, if $\bar{r}/\bar{\kappa}$ is much larger than 1, it indicates a length distribution that is dominated by catastrophe and turnover. In metaphase (Fig 6A, B, E, F, Suppl. Fig. 1 A,B,E,F) and early anaphase (Fig. 6C, G, Suppl. Fig. 1 C,G) we find that the non-dimensionalized turnover rate $\bar{r} = r/v_g\ell$ is equal to 1.0, while the non-dimensionalized cutting rate $\bar{\kappa} = \kappa/v_g\ell^2$ is about 0.1. Here, ℓ is the average microtubule length. These numbers imply that the length at which a microtubule is more likely to be cut than to undergo catastrophe is $\bar{r}/\bar{\kappa} \simeq 10$, *i.e.*, cutting is a relatively rare event. In fact, there are no microtubules in metaphase that are longer than 10 times the average microtubule length $\ell = 1\mu\mathrm{m}$ (*i.e.*, 10 µm) and only 1 microtubule was larger than *10 times the average length* $\ell = 0.5\mu\mathrm{m}$ (*i.e.*, 5 µm) in early anaphase. This also implies that the change in the microtubule length observed from metaphase (ℓ = 1 µm) to early anaphase (ℓ = 0.5 micron), is a consequence of either the microtubule turnover rate, or changes in microtubule growth velocity. For error estimates and detailed likelihood plots of the inferred parameters see Fig. 6 and Suppl. Fig.1, which give 95% confidence intervals and likelihood surfaces for all parameters. Note also that given that cutting occurs very rarely the inference is not informative on the parameter α, which describes the stability of newly cut microtubules.

We next use our estimate for the ratio $\bar{r} = r/v_g\ell$ to infer the microtubule growth velocity in meiotic metaphase spindles. For this we took the measured FRAP half-life in metaphase (see Fig 2B) of about 5 s as an estimate for microtubule turnover time 1/r and determine the average microtubule length of about 1 µm (Table 1). Using these values, we estimated that the microtubule growth velocity (vg) during metaphase was close to 12 µm/min. Interestingly, this agrees with growth velocity estimates based on microtubule flux, and it is similar to values reported for microtubule growth rates in the dense regions of mitotic *C. elegans* spindles, reaching from 16-20 µm/min (Redeman et al 2017). Notably, this value is slower than growth rates reported for astral microtubules (44 µm/min) growing away from centrosomes reported by Redeman et al 2017 and Srayko et al 2005. This suggests that microtubule growth velocities

are under spatial and temporal control within the cytoplasm, as was previously described by (Geisterfer et al 2019, Walczak et al 2016)

The drastic change in the average microtubule length from metaphase to anaphase could be due to a decrease in microtubule growth velocity to half its metaphase value (6 µm/min). Alternatively, it could also be caused by an increase in microtubule turnover rate. Given the large relative errors of the FRAP measurements in the very small meiotic spindles, we cannot definitely answer whether microtubule growth speed, turnover rate, or both are under biochemical control at this stage. In toto, our data argue that the transition from metaphase to early anaphase is best explained by modulating microtubule growth and polymerization dynamics, and not by increased microtubule cutting. Note that a role for katanin in amplification of microtubule mass and number has been suggested *in vitro*, where severing activity can result in the incorporation of GTP-tubulin into the microtubule lattice, thus increasing the rescue frequency and stability of newly emerging microtubule ends (Vemu et al 2018).

We finally asked the same question for the transition from early to mid anaphase. We find that later in anaphase the relative importance of cutting increases with $\bar{\kappa}$ = 0.3, and $\bar{r}$ = 0.9, see Fig 6D, H. This means that, at this later point, the length at which a microtubule is more likely to be cut than to undergo catastrophe decreases to 3 ℓ, which would be approximately 3% of the microtubule population.

Thus, our data suggest that the initial steps of the transition from metaphase to anaphase are due to changes in microtubule turnover rate and growth and not mediated by katanin dependent severing. This is surprising since earlier work clearly demonstrated the importance of severing during spindle assembly (Srayko et al 2006, McNally et al 2011, McNally et al 2014, Connolly et al 2014, Joly et al 2016). Estimates of the number of Katanin-mediated cutting events by counting lateral defects in partial EM reconstructions of meiotic spindles at earlier stages had found a large number of cutting events in wildtype spindles (Srayko et al 2006). To test the predictions of our inference scheme we decided to look for similar cutting sites in our datasets.

Analyzing the frequency of lateral defects in our tomographic data, indicated a very low abundance (1.1% of microtubules in Metaphase #2, 2.5% in early anaphase and 1.8% in mid Anaphase). We could also not detect an increased occurrence of lateral defects in longer microtubules or at distinct positions within the

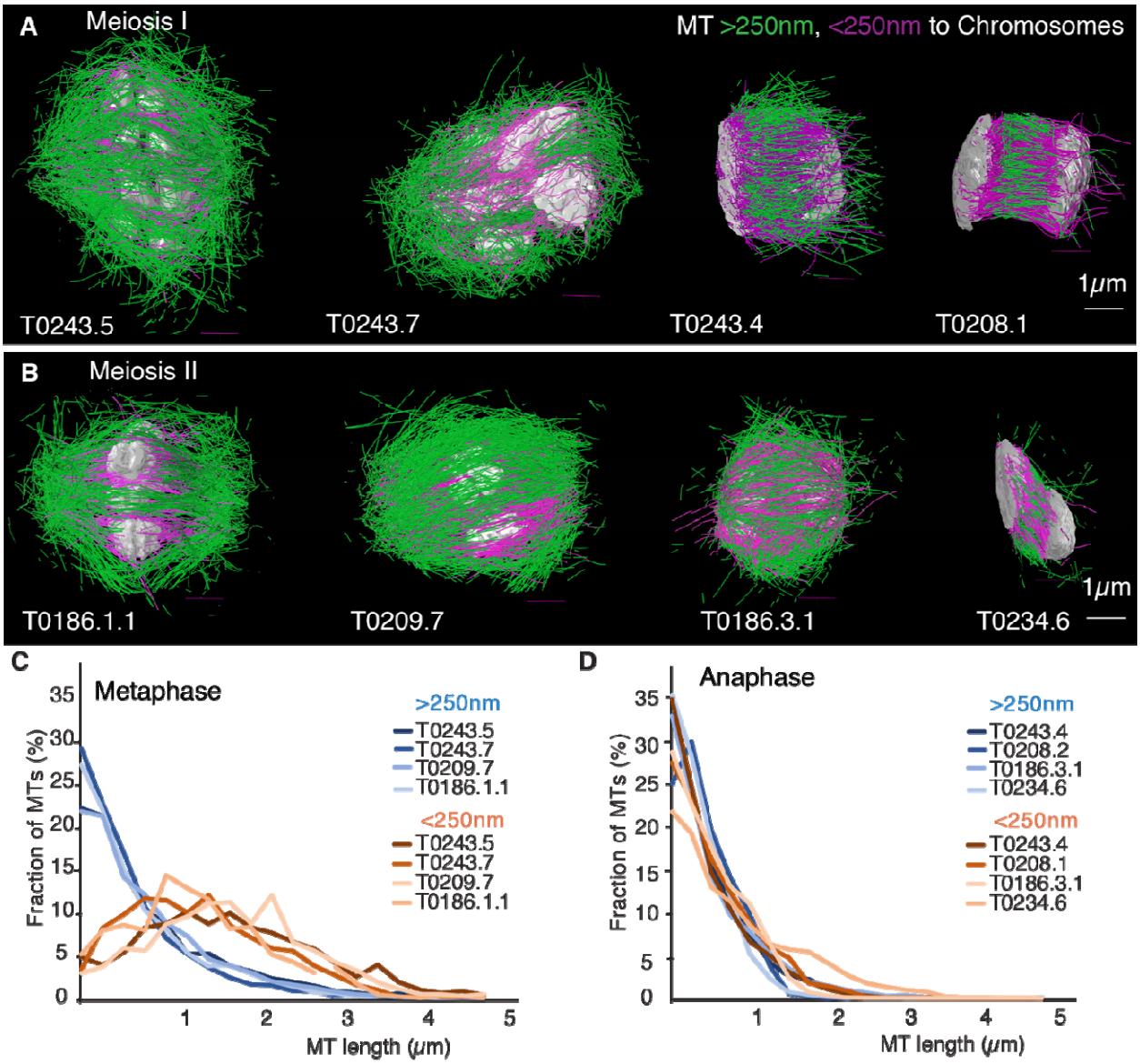

Figure 7

Figure 7. Analysis of microtubule length distributions within 150nm of the chromosomes.
A*, Tomographic reconstructions of meiotic spindles in meiosis I from metaphase to anaphase. The reconstructions show microtubules located with and end or lattice point within 150nm from the chromosome surface in magenta and microtubules located further away in green. Chromosomes are grey. Scale bar 1µm.* ***B****, Same as* ***A*** *but for spindles in meiosis II.* ***C****, Plot of the length distribution of microtubules in respect to their distance from the chromosomes for metaphase spindles in meiosis I and*

II. Red lines show microtubules located within 150nm from the chromosomes, blue lines show microtubules further away. Bin size 250nm. ***D****, Similar to plot in* ***C*** *but for anaphase spindles in meiosis I and II.*

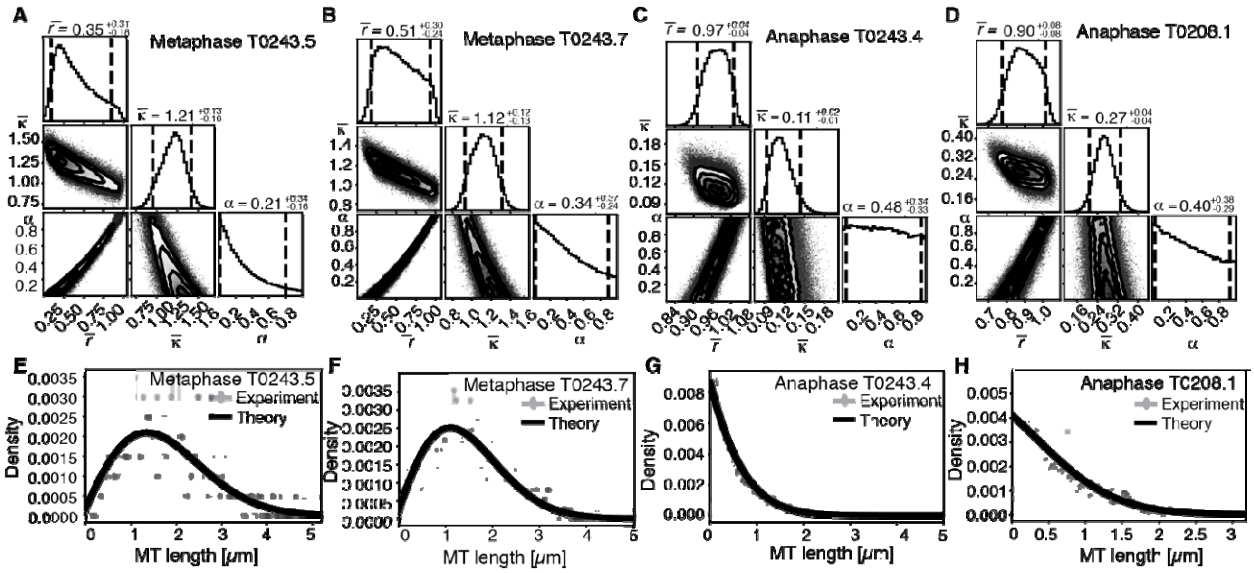

Figure 8

Figure 8. Selective inference model parameters in metaphase and anaphase spindles for microtubules located within 150nm of the chromosomes

A*, Likelihood distribution of model parameters determined by Markov Chain Monte-Carlo for microtubules within 150nm distance from the chromosomes in Metaphase T0243.5 meiosis I. The top boxes show the totally marginalized distribution of parameters, with dashed lines delimiting the 95% confidence interval. Surface plots show cuts through the likelihood distributions, marginalized onto 2D subspaces. Lines are contour lines, dots indicate MCMC-samples.* ***B****, Same as in* ***A*** *but for meiosis I metaphase T0243.7 dataset.* ***C****, Same as in* ***A*** *but for meiosis I T0243.3 early Anaphase dataset.* ***D****, Same as in* ***A*** *but for the meiosis I mid Anaphase T0208.1 dataset* ***E, F, G, H*** *Comparison of experimentally determined length distributions of microtubules located within 150nm from the chromosome surface (dots) to the prediction of the highest likelihood model (solid line) for meiosis I Metaphase T0243.5 (****E****), meiosis I Metaphase T0243.7 (****F****), meiosis I early Anaphase T0234.4 (****G****) and meiosis I mid Anaphase T0208.1 (****H****). Plots for meiosis II can be found in Supplementary Figure 2.*

spindle. This is notably fewer events than what was reported for earlier spindles. We conclude that the initial steps of the transition from metaphase to anaphase are due to changes in microtubule turnover rate and growth and not mediated by katanin dependent severing.

Cutting selectively occurs for microtubules in close chromosome contact

Our finding that global rearrangements of the spindle structure are mainly caused by changes in nucleation and turnover dynamics, made us wonder about the role of katanin-mediated cutting in these spindles. To investigate this, we separated out microtubules in close contact to chromosomes (defined as being closer than 150 nm) (Fig. 7A, B) and analyzed them separately using our inference scheme. The results are shown in Figure 8 and Suppl. Fig. 2. In metaphase spindles the fraction of microtubules in close contact to chromosomes is small. We found 13%, 25%, 16%, 23% for our four Metaphase spindle datasets, respectively. However, in contrast to the global population, they showed strong evidence of cutting and $\bar{\kappa} > 1$ in all four examples. Furthermore, the length distribution of these microtubules, as depicted in Fig 7C and Fig. 8 E, F and Suppl. Fig. 2 E,F, is clearly not exponential in metaphase, which is also indicative of cutting.

In contrast, in anaphase, the majority of microtubules (about 70%) are in close contact to chromosomes. Despite this, even MTs in close contact with chromosomes showed a nearly exponential length distribution (Fig. 7D, Fig. 8 G,H, Suppl. Fig. 2 G,H), and our inference scheme yields the same results for MTs near chromosomes and the global MT population. The plots for microtubules that were located further than 150 nm are comparable to the plots for all microtubules (Fig.6) and are shown in supplementary Figure 3.

Together, these data suggest a role for cutting in maintaining the metaphase spindle. In particular we hypothesize that Katanin selectively cuts microtubules that are in close contact with chromosomes. This mechanism seems to be suppressed in late anaphase.

Katanin depletion reduces the fraction turn-over but not the turn-over rate of microtubules

We next sought to investigate the role of katanin on microtubule turn-over in the metaphase spindle. As null mutants of the *C. elegans* katanin homologs MEI-1 and MEI-2 do not assemble bipolar spindles

(Mains et al 1990), we decided to work with the FM13 *mei-2(ct98)* strain, which has an overall lower expression of MEI-2 (Srayko et al 2000) and reduced microtubule-severing activity (McNally et al 2006, McNally et

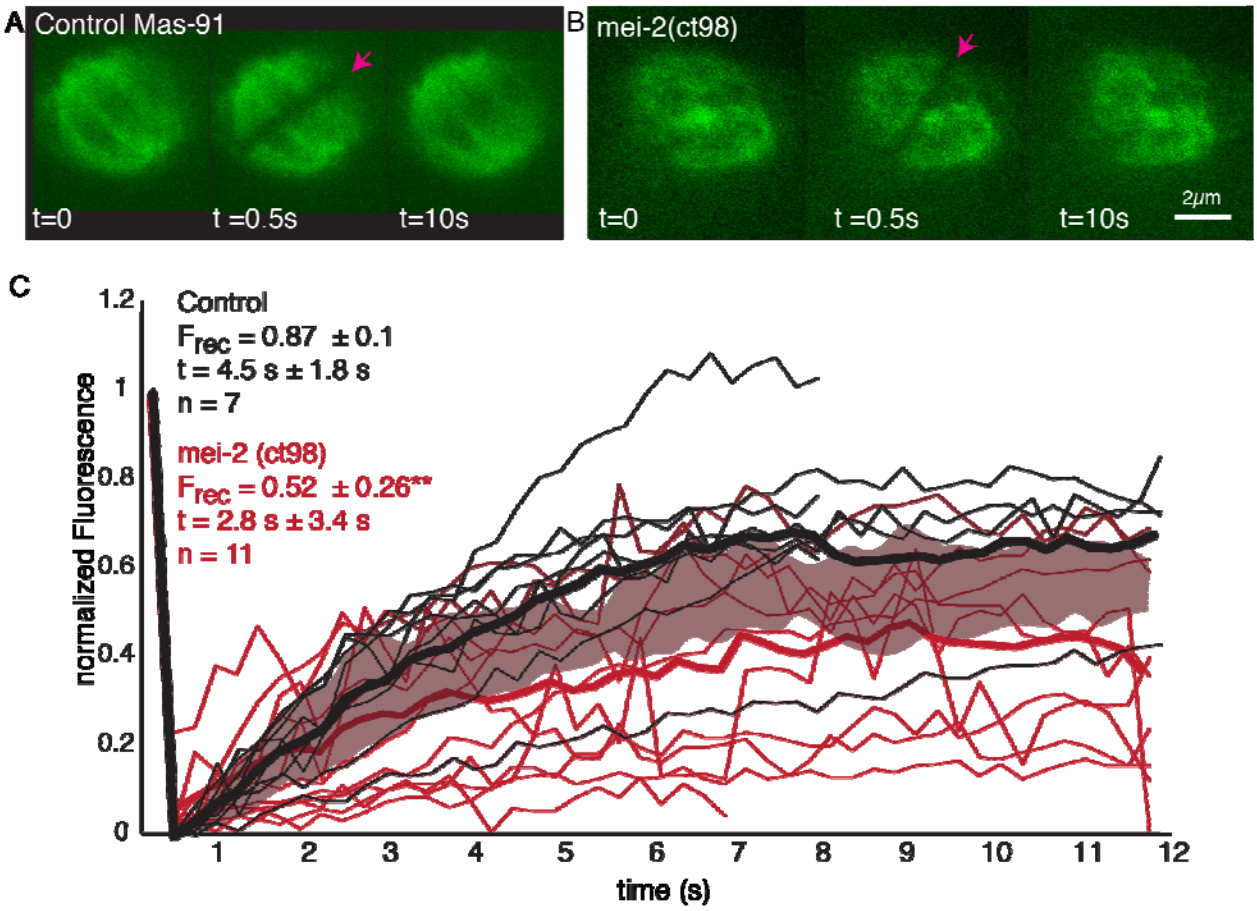

Figure 9

Figure 9. Microtubule turn-over during metaphase of meiosis I in mei-2(ct98) embryos.

A*, Light microscope images of spindles in control embryos in meiosis I prior to and after photo bleaching at the spindle center (red arrow). The time points are indicated.* ***B****, Light microscope images of spindles in meiosis I in the katanin mei-2(ct98) mutant prior to and after photo bleaching at the spindle center (red arrow). The time points are indicated. Scale bar 2µm* ***C****, Plot of the recovery of the bleach mark over time in control embryos (black) and mei-2 (ct98) (red) for different datasets. Mean values are indicated by thick lines, the shaded region corresponds to the standard deviation. The fraction of recovery (F_{rec}) and recovery times for the data sets are shown in the plot.*

al 2014). We used FRAP experiments to measure the effect of katanin mutation on microtubule turn-over using the FM13 *mei-2(ct98)* strain (Fig. 9 A, B). We found that the characteristic time-scales for recovery

were not significantly affected (4.5 s ± 1.8 s (n=7) in control and 2.8 s ± 3.4 s (n=11) in mei-2(ct98), p = 0.2434). However, strikingly we observed a significant decrease in the fraction of fluorescence recovery of microtubules in the mei-2(ct98) embryos (Fig.9 C). While in wild-type embryos, 87 % ± 10 % of the fluorescent tubulin signal recovers, this is significantly reduced to 52% ± 26% (p = 0.0039) in the katanin mutant. This suggests the presence of a population of stabilized microtubules in katanin-depleted spindles. In line with other authors (Brinkley and Cartwright 1975, Rieder et al 1981, Bakhoum et al 2009) we thus speculate that microtubules in close contact to chromosomes get stabilized by interacting with the chromosomes. Katanin keeps these microtubules from growing too long by cutting these microtubules, and

thus, effectively enhances turn over in spindles. In line with this model, our inference data (Fig. 8) suggests the new plus ends of newly cut MTs are mostly unstable. In line with this model our inference scheme predicts values for α that are smaller than 0.5 for chromosome proximal microtubules in all four metaphase spindles.

However, given the small number of microtubules in close contact to chromosomes, some significant uncertainty on this number remains.

Discussion

Acentrosomal meiotic spindles in *C. elegans* undergo a reorganization from a bipolar microtubule arrangement in metaphase to an inter-chromosomal microtubule array in anaphase. Along with this microtubule reorganization, chromosomes are segregated to extrude half of the genetic material as polar bodies. The underlying mechanism of the microtubule reorganization is not very well understood, and several mechanisms could be involved, for instance katanin-mediated severing as reported for *C. elegans* meiosis I (Joly et al 2016, Srayko et al 2006), transport of microtubules as reported for *C. elegans* and Xenopus meiotic spindles (Mullen & Wignall 2017, Brugués et al 2012) or changes in microtubule polymerization dynamics a shown for Xenopus meiotic spindles (Brugués et al 2012, Needleman et al 2010). Here we have generated complete 3D reconstructions of meiotic spindles in *C. elegans* at different

stages and combined this ultrastructural analysis with light microscopy and simulations to investigate the rearrangement of microtubules during meiosis.

Based on light microscopy, previous publications suggested that the microtubule rearrangement from metaphase to anaphase in meiosis I and II in *C. elegans* could be driven by an initial inward sliding of antiparallel microtubules by kinesin 14 family members (McNally 2016) and a subsequent depolymerization of microtubules at the spindle pole, due to severing by katanin (McNally 2006). This was based on the observation that the initial phase of spindle shortening is accompanied by an increase of microtubule density, followed by a further shortening and depolymerization of microtubules at the spindle poles, resulting in a decrease of microtubule density. In agreement with this, our tomographic reconstructions show an initial increase in microtubule number and density during early anaphase, which is followed by a decrease in microtubule number and density in mid anaphase. However, while inward sliding of microtubules would result in an increased density, it does not explain the observed 2-fold increase of microtubule number. In addition, our data showed a poleward-directed movement of microtubules, contradicting an inward sliding. This suggests that inward sliding is unlikely to contribute to spindle shortening and cannot account for the appearance of microtubules between the chromosomes that characterizes anaphase.

The reorganization of microtubules could alternatively be driven by a selective depolymerization of microtubules at the spindle poles. However, our data suggests that the spindle rearrangement is mainly driven by changes in microtubule nucleation and turn-over. A more local analysis of the changes in microtubule length and number, which revealed differences between microtubules near the chromosomes (within 150nm) and those further away (Fig.7), as well as investigations of local changes using the mathematical model (Fig. 8) showed spatial differences in microtubule properties and dynamics.

Our data showed that spindles are made from arrays of dynamic short microtubules, that turnover within 5 seconds. We further showed that the dramatic structural rearrangements observed from metaphase to anaphase are correlated with drastic changes in the microtubule number and length distribution. Meiotic

metaphase spindles are composed of fewer but longer microtubules, while spindles in early anaphase are made of more but shorter microtubules.

These observations led us to ask whether severing of microtubules by katanin, or an increase in microtubule dynamics, allowing more nucleation and/or higher rates of catastrophe, would better explain our observations. For this we developed a mathematical model that predicts the microtubule length distribution from cutting rates and turnover dynamics. We inferred parameters for the model using the microtubule length distribution and numbers found in electron tomography. This analysis severely constrains the possible mechanisms for spindle restructuring from metaphase to anaphase. Our data suggest that cutting of microtubules in the vicinity of chromosomes is important for maintaining metaphase spindles. It is tempting to speculate that microtubules near the chromosomes are more stable, similar to kinetochore microtubules in mitosis and that katanin supports the turn-over of those more stable microtubules by severing. For the transition from metaphase to anaphase however, cutting seems to play less of a role. Globally the fraction of microtubules that show signs of cutting is small. Moreover, cutting seems to be much less prominent, even in chromosome proximal MTs during anaphase.

Interestingly, a role for microtubule severing proteins, including katanin, in microtubule amplification has recently been suggested based on in vitro studies. Here, katanin induces nanoscale damage to the microtubule lattice, resulting in the incorporation of GTP tubulin (Vemu et al 2018, Schaedel et al 2015, 2019) and stabilization of microtubules. The incorporation of GTP-tubulin into the lattice is thought to have two effects: promoting rescue as well as the stability of a new plus-end formed upon severing. This would result in an amplification of microtubules. Consistent with this, our data shows a two-fold increase of microtubule number during the transition from metaphase to early anaphase. Similarly, Srayko *et al* 2006 reported a decrease in microtubule number in *C. elegans* embryos depleted of katanin.

In summary, by combining light microscopy with electron tomography and mathematical modeling we analyzed the reorganization of microtubules during the transition from metaphase to anaphase in *C. elegans* meiotic embryos. Our data suggests that this reorganization is driven by changes in microtubule

growth and/or turn-over and that katanin promotes microtubule turn-over by severing microtubules near the chromosomes.

Acknowledgements

The authors are thankful to Th. Müller-Reichert for continuous support and to S. Tulok and Dr. A. Walther (Core Facility Cellular Imaging, Faculty of Medicine Carl Gustav Carus, TU Dresden) for help with light microscopy. The authors are also grateful to the members of the electron and light microscopy facility at the Max Planck Institute of Molecular Cell Biology and Genetics (MPI-CBG, Dresden) for technical assistance, J. Baumgart (MPI-PKS, Dresden) for initial help in data analysis and F. McNally (UC Davis) for the *mei-2(ct98) C. elegans* strain. The authors would like to thank Drs. E. O'Toole and R. McIntosh (Boulder) for a critical reading of the manuscript. Ina Lantzsch and Erik Szentgyörgyi were supported by funds from the Deutsche Forschungsgemeinschaft (MU 1423/3-1, 3-2 and 8-1 to T. Müller-Reichert) and the Human Frontier Science Programme (RGP 0034/2010 to D. N. and T.M.R). S. Redemann received funding from the Faculty of Medicine Carl Gustav Carus of the TU Dresden (Frauenhabilitationsstipendium).

Materials and methods

Worm strains and gene silencing by RNAi

Worm strains

The following *C. elegans* strains were used in this study: strain MAS91 (unc-119(ed3) III; ItIs37[pAA64; pie-1::mCherry::HIS58]; ruIs57[pie-1::GFP::tubulin + unc-119(+)]) for live-cell imaging and correlative light microscopy/electron tomography, strain SA250 (tjIs54 [pie-1p::GFP::tbb-2 + pie-

1p::2xmCherry::tbg-1 + unc-119(+)]; tjIs57 [pie-1p::mCherry::his-48 + unc-119(+)]), MAS91 and FM13 (*mei-2(ct98) I*; *ruls57 [pAZ147: pie-1^{promoter}::tubulin::GFP; unc-119 (+)]*; *itls37 [unc-119(+) pie-1^{promoter}::mCherry::H2B]*; *him-8(e1489) IV)*, for FRAP experiments. Strains were cultured and maintained at 16°C as described (Brenner, 1974).

Light microscopy

Sample preparation for light microscopy

Oocytes for live-cell imaging were prepared as described previously (Woog et al., 2012). For FRAP measurements, meiotic spindles in oocytes were observed in the uterus of adult hermaphrodites (strain SA250) mounted on a thin 4% Agarose pad between a slide and a coverslip. Polystyrene microspheres (Microspheres 0.10 μm, Polysciences, Inc.) were added to the agar solution before specimen mounting to immobilize the living worms.

Spinning disk confocal fluorescence imaging

Live imaging was performed using a spinning disk confocal microscope (Nikon Ti2000, Yokugawa CSU-X1), equipped with 488-nm and 561-nm diode lasers, an EMCCD camera (Hamamatsu), and a 60X water-immersion objective (CFI Plan Apo VC 60X WI, NA 1.2, Nikon). Acquisition parameters were controlled using a home-developed LabVIEW program (LabVIEW, National Instruments). Images were acquired every 1 second with a single z-plane.

FRAP experiments

The photobleaching system was constructed on the above-mentioned spinning disk confocal microscope. 80-MHz femtosecond pulsed laser with 0.3-nJ pulse energy and 800-nm center wavelength was used for performing photobleaching and generated from a Ti:sapphire pulsed laser (Mai-Tai, Spectra-Physics, Mountain View, CA). The photobleaching laser was focused through the same objective for imaging, and photobleaching was performed by moving the sample on a piezo-stage (P-545 PIano XYZ, Physik Instrumente) in three dimensions controlled by a home-developed LabVIEW program (LabVIEW,

National Instruments). Scanning line-bleaching with z-steps were created by moving the stage perpendicular to the pole-to-pole axis back and forth on the focal plane while lowering the stage in the z direction. The parameter for bleaching in length by depth was 6 x 2 µm. The moving speed of the stage was 50 µm/sec.

mei-2(ct98) FRAP experiment

Worms from the *mei-2(ct98ts)* strain as well as MAS-91 worms were kept at 16 degree until the time of imaging. The FRAP experiment was conducted using a Yokogawa CSU-W1 SoRa dual cam spinning disk confocal. This microscope is equipped with seven lasers for imaging (405, 445, 488, 514, 561, 594, 640 nm) that allow near-optimal excitation of common fluorescent proteins and minimize crosstalk. This spinning disk confocal is mounted on a Nikon Ti2 inverted microscope with a motorized stage for time-lapse imaging of multiple stage positions, piezo z-drive for rapid z-stack acquisition, and a Perfect Focus module to compensate for stage drift during time-lapse imaging. For image acquisition, the microscope is equipped with two types of cameras optimal for different types of experiments, which are mounted on the two camera ports of the CSU-W1 dual cam head: (1) a Hamamatsu ORCA Fusion camera for high-resolution imaging; and (2) dual Photometrics Prime 95B cameras on a Cairn TwinCam for higher speed imaging and/or simultaneous acquisition of two channels. Hardware triggering allows rapid acquisition of z-stacks. The microscope is equipped with an Acal BFi UV Opti-Microscan point scanner that we used for the FRAP experiment. This system is integrated with Nikon NIS Elements software for seamless experimental setup and data acquisition. The movies were acquired with a 60x 1.27NA water objective and 2.8x SoRa magnifier with 100 msec exposure times and 250 msec intervals (4 frames/sec).

Analysis of fluorescence recovery after photobleaching and microtubule poleward flux

Fluorescence recovery after photobleaching (FRAP) and rate of microtubule poleward flux was calculated with a combination of Fiji (Schindelin et al., 2012) and Matlab (MATLAB and Statistics Toolbox Release 2012, The MathWorks, Nitick, USA). Time-lapse images of spindles expressing GFP::tubulin and

mCherry::histone (corresponding to chromosomes) were realigned in a routine for matching, rotation and translation using Rigid Body of Fiji's StackReg plug-in, so that the random displacement of the spindle due to the spontaneous motion of the worm was corrected.

Poleward flux and recovery of photobleached makers were tracked using a program written in Matlab (MATLAB and Statistics Toolbox Release 2012, The MathWorks, Nitick, USA). Line-scans of GFP-labeled tubulin along the metaphase spindle were extracted over the course of anaphase. To track the microtubule poleward flux, each line-scan at each time point can be divided into two halves by the middle plane of the spindle. The half of the line profile with the bleached mark was subtracted from the other half of the non-bleached profile by a reflection of symmetry around the middle plane of the spindle. This profile subtraction was used to remove spatial variations in the background fluorescence, a valid procedure assuming mirror symmetry of the spindle around its middle plane. A Gaussian function was used to fit the subtracted profile to locate the center of the bleached mark, and thus the position of the bleached mark versus time was extracted. A straight line was fitted to the position of the bleached mark versus time to retrieve the rate of the bleached mark. The recovery time of GFP::tubulin after photobleaching was determined by using an exponential fit. The fluorescence intensities of photobleached marks were calculated by summing intensities over 3 pixels (~0.5 μm) around the center of the photobleach mark.

Electron microscopy

Sample preparation

Samples for electron tomography were prepared as described (Woog et al., 2012). Briefly, hermaphrodites were dissected in Minimal Edgar´s Growth Medium (Edgar, 1995) and embryos in early meiosis were selected and transferred to cellulose capillary tubes (Leica Microsystems, Vienna, Austria) with an inner diameter of 200 μm. The embryos were observed with a stereomicroscope, transferred to membrane carriers at appropriate stages and immediately cryo-immobilized using an EMPACT2 high-

pressure freezer (Leica Microsystems, Vienna, Austria) equipped with a rapid transfer system (Pelletier et al., 2006). Freeze substitution was performed over 3 d at -90°C in anhydrous acetone containing 1% OsO_4 and 0.1% uranyl acetate using an automatic freeze substitution machine (EM AFS, Leica Microsystems, Vienna, Austria). Epon/Araldite infiltrated samples were then embedded in a thin layer of resin and polymerized for 3 d at 60°C. Embedded embryos were re-mounted on dummy blocks and serial semi-thick (300 nm) sections were cut using an Ultracut UCT Microtome (Leica Microsystems, Vienna, Austria). Sections were collected on Formvar-coated copper slot grids and post-stained with 2% uranyl acetate in 70% methanol followed by Reynold's lead citrate.

Electron tomography

For dual-axis electron tomography (Mastronarde et al 1997), 15-nm colloidal gold particles (Sigma-Aldrich) were attached to both sides of semi-thick sections to serve as fiducial markers for subsequent image alignment. Series of tilted views were recorded using a TECNAI F30 transmission electron microscope (FEI Company, Eindhoven, The Netherlands) operated at 300 kV. Images were captured every 1.0° over a ± 60° range at a pixel size of 2.3 nm using a Gatan US1000 2K x 2K CCD camera. Using the IMOD software package, a montage of 2 x 1 [meiosis I: metaphase #1, metaphase #2, anaphase (late) #1, anaphase (late) #2; meiosis II: metaphase #1, metaphase #2] or 2 x 2 [meiosis I: anaphase (early); meiosis II: anaphase (late)] frames was collected and combined for each serial section to cover the lengths of the meiotic spindles (Kremer et al., 1996; Mastronarde, 1997).

For image processing the tilted views were aligned using the positions of the fiducials. Tomograms were computed for each tilt axis using the R-weighted back-projection algorithm (Gilbert, 1972). In order to cover the entire volume of each spindle, we acquired tomograms of about 8-12 consecutive sections per sample. In total, we recorded 10 wild-type spindles in meiosis I and II (Supplementary Table 1 and 2).

Three-dimensional reconstruction and automatic segmentation of microtubules

We used the IMOD software package (http://bio3d.colorado.edu/imod) for the calculation of electron tomograms (Kremer et al., 1996). We applied the Amira software package for the segmentation and automatic tracing of microtubules (Stalling et al., 2005). For this, we used an extension to the filament editor of the Amira visualization and data analysis software (Redemann et al., 2017; Redemann et al., 2014; Weber et al., 2012). We also used the Amira software to stitch the obtained 3D models in *z* to create full volumes of the recorded spindles (Redemann et al., 2017; Weber et al., 2014). The automatic segmentation of the spindle microtubules was followed by a visual inspection of the traced microtubules within the tomograms. Correction of the individual microtubule tracings included: manual tracing of undetected microtubules, connection of microtubules from section to section and deletions of tracing artifacts (e.g. membranes of vesicles). Approximately 5% of microtubules needed to be corrected (Redemann et al., 2017).

Data and error analysis

Data analysis was performed using either the Amira software package or by exporting the geometric data of the traced microtubules followed by an analysis using MatLab (MATLAB and Statistics Toolbox Release 2012, The MathWorks, Nitick, USA). In our analysis of spindle structure, the following errors were considered (Redemann et al., 2017). Briefly, during the data preparation and the imaging process, the tomograms are locally distorted. Furthermore, the exposure of the electron beam causes a shrinking of the sample. During the reconstruction of the microtubules, however, the most important errors occur in the tracing and matching process. In addition, the data is again distorted in all directions to align the tomograms. We assumed that this distortion primarily compensates the distortion of the imaging process. For the tracing, the error was previously analyzed for reconstructions of *C. elegans* centrosomes (Weber et al., 2012). We assumed that the error lies in the same range of 5-10%. In addition, the traced microtubules were manually verified. It is more difficult to estimate the error of the matching algorithm (Weber et al., 2014), since it depends on the local density and properties of the microtubules. The quality of our analysis should be influenced only by minor 3D distortions.

Quantification of tomographic data

Microtubule length and positioning

The reconstruction algorithm for microtubules in serial-section electron microscopy represents each microtubule as a 3D piecewise linear curve of its centerline. Thus, the length of the microtubule is given by the sum of the lengths of the line segments.

Supplementary movies

Suppl. Movie 1. **Visualization of spindle ultrastructure in meiosis I at mid anaphase**

This movie (corresponding to Figure 1A; anaphase, mid) shows a close up-view of the microtubule organization at mid anaphase. Microtubules are visualized in green, chromosomes in grey.

Suppl. Movie 2. **Visualization of spindle ultrastructure in meiosis I at late anaphase**

This movie (corresponding to Figure 1A; anaphase, late #1) shows a close up-view of the microtubule organization at late anaphase. Microtubules are visualized in green, chromosomes in grey.

Suppl. Movie 3. **Visualization of spindle ultrastructure in meiosis I at late anaphase**

This movie (corresponding to Figure 3A; anaphase, late #2) shows a close up-view of the microtubule organization at late anaphase. Microtubules are visualized in green, chromosomes in grey.

Suppl. Movie 4. FRAP during metaphase in Meiosis I in control embryo

Movie of a FRAP experiment during metaphase in meiosis I of *C. elegans* expressing GFP tubulin and mCherry Histone. A small stripe is bleached next to the Chromosomes (right side) and the motion and recovery of the stripe over time are analyzed. Framerate 1fps.

Suppl. Movie 5. FRAP during metaphase in Meiosis I in *mei-2(ct98)* embryo

Movie of a FRAP experiment during metaphase in meiosis I of *C. elegans mei-2(ct98)* expressing GFP tubulin and histone cherry. Only the tubulin channel is shown. A small stripe is bleached in the center of the spindle and recovery of the stripe over time is analyzed. Framerate 5 fps.

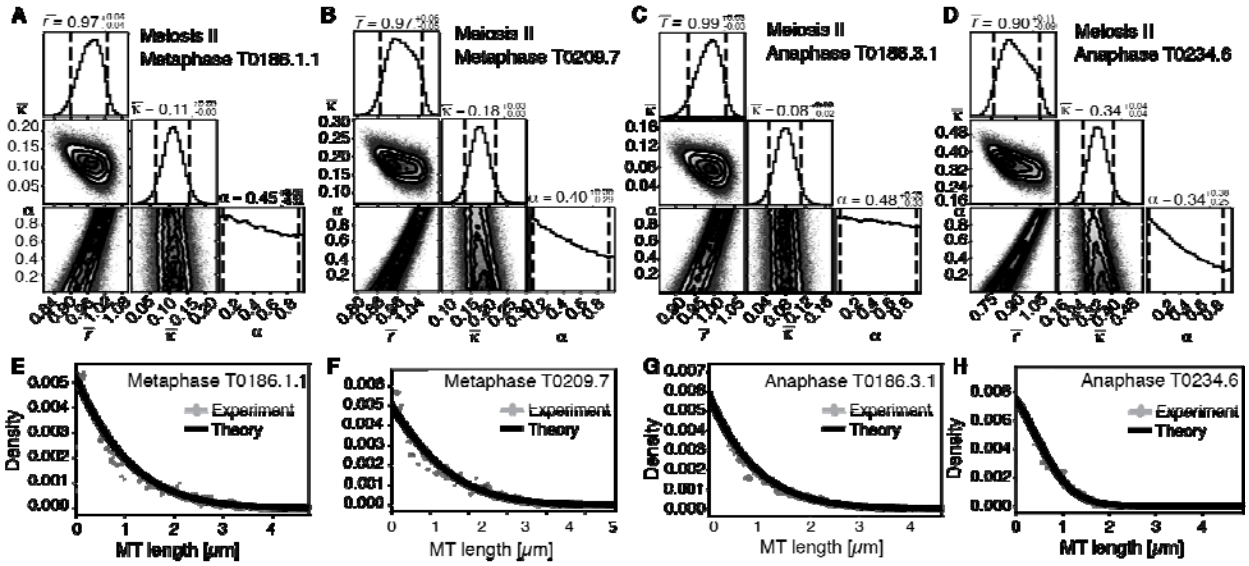

Supplementary Figure 1. Selective inference model parameters in metaphase and anaphase spindles for microtubules in meiosis II

A, Likelihood distribution of model parameters determined by Markov Chain Monte-Carlo for meiosis II Metaphase T0186.1.1. The top boxes show the totally marginalized distribution of parameters, with dashed lines delimiting the 95% confidence interval. Surface plots show cuts through the likelihood distributions, marginalized onto 2D subspaces. Lines are contour lines, dots indicate MCMC-samples. **B**, Same as in **A** but for the Metaphase T0209.7 dataset. **C**, Same as in **A** but for the early Anaphase T0186.3.1 dataset. **D**, Same as in **A** but for the mid Anaphase T0234.6 dataset.

E, F, G, H Comparison of experimentally determined length distribution of microtubules (dots) to the prediction of the highest likelihood model (solid line) for Metaphase T0186.1.1 (**E**), Metaphase T0209.7 (**F**), early Anaphase T0186.3.1 (**G**) and mid Anaphase T0234.6 (**H**).

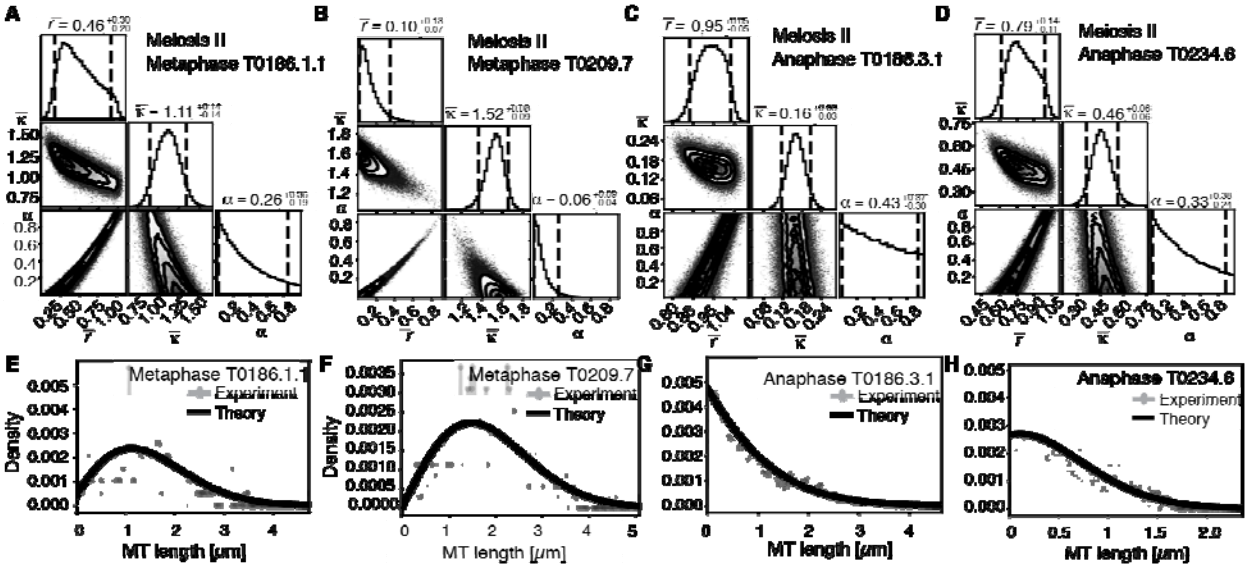

Supplementary Figure 2. Selective inference model parameters in meiosis II metaphase and anaphase spindles for microtubules located within 150nm of the chromosomesocated
A, Likelihood distribution of model parameters determined by Markov Chain Monte-Carlo for microtubules within 150nm distance from the chromosomes in meiosis II Metaphase T0186.1.1. The top boxes show the totally marginalized distribution of parameters, with dashed lines delimiting the 95% confidence interval. Surface plots show cuts through the likelihood distributions, marginalized onto 2D subspaces. Lines are contour lines, dots indicate MCMC-samples. **B**, Same as in **A** but for the Metaphase T0209.7 dataset. **C**, Same as in **A** but for the early Anaphase T0186.3.1 dataset. **D**, Same as in **A** but for the mid Anaphase T0234.6 dataset. **E, F, G, H** Comparison of experimentally determined length distribution of microtubules (dots) to the prediction of the highest likelihood model (solid line) for Metaphase T0186.1.1 (**E**), Metaphase T0209.7 (**F**), early Anaphase T0186.3.1 (**G**) and mid Anaphase T0234.6 (**H**).

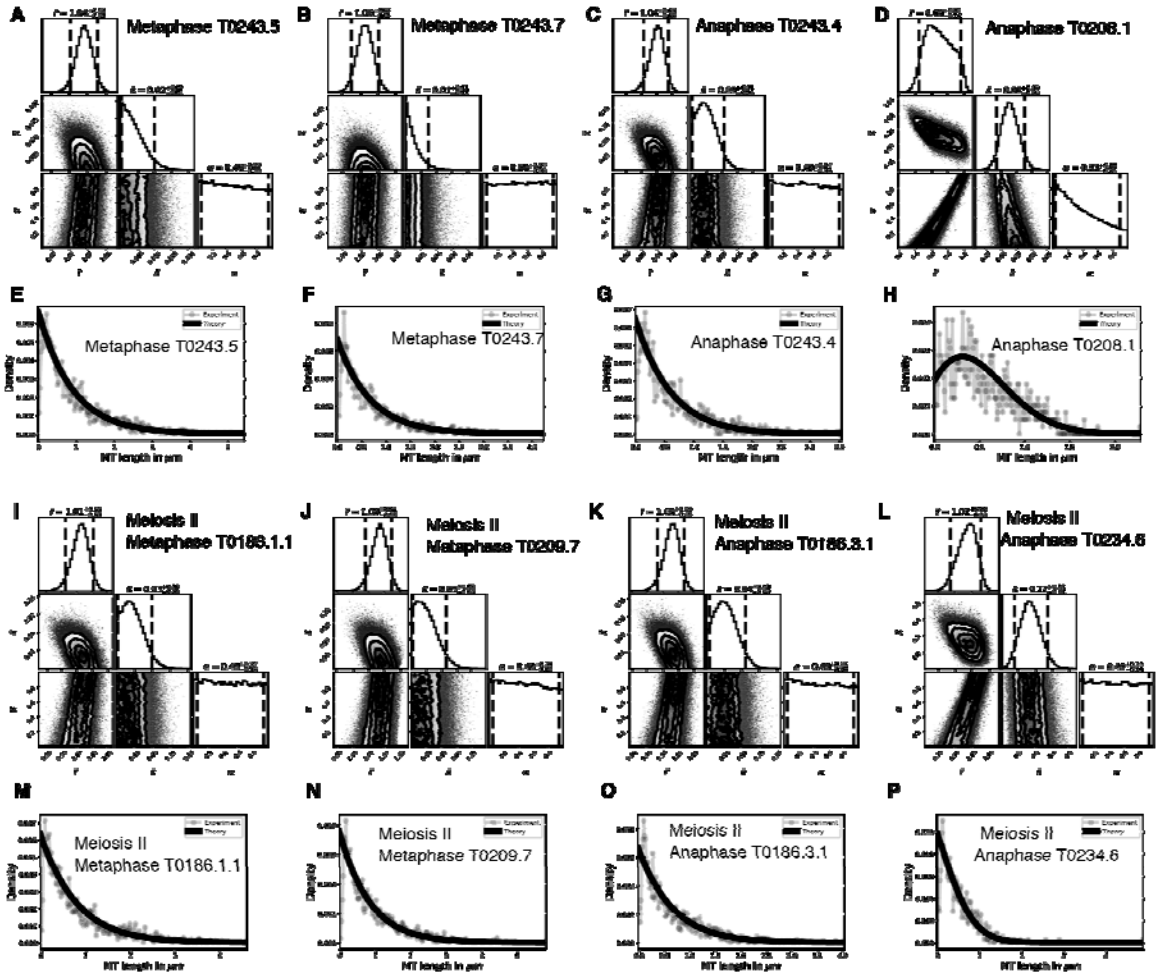

Supplementary Figure 3. Selective inference model parameters in metaphase and anaphase spindles for microtubules located further than 150nm from the chromosomes in meiosis I and II

A, Likelihood distribution of model parameters determined by Markov Chain Monte-Carlo for meiosis II Metaphase T0186.1.1. The top boxes show the totally marginalized distribution of parameters, with dashed lines delimiting the 95% confidence interval. Surface plots show cuts through the likelihood distributions, marginalized onto 2D subspaces. Lines are contour lines, dots indicate MCMC-samples. **B**, Same as in **A** but for the Metaphase T0209.7 dataset. **C**, Same as in **A** but for the early Anaphase T0186.3.1 dataset. **D**, Same as in **A** but for the mid Anaphase T0234.6 dataset.

E, F, G, H Comparison of experimentally determined length distribution of microtubules (dots) to the prediction of the highest likelihood model (solid line) for Metaphase T0186.1.1 (**E**), Metaphase T0209.7 (**F**), early Anaphase T0186.3.1 (**G**) and mid Anaphase T0234.6 (**H**).

I, Likelihood distribution of model parameters determined by Markov Chain Monte-Carlo for microtubules within 150nm distance from the chromosomes in meiosis II Metaphase T0186.1.1. The top boxes show the totally marginalized distribution of parameters, with dashed lines delimiting the 95% confidence interval. Surface plots show cuts through the likelihood distributions, marginalized onto 2D subspaces. Lines are contour lines, dots indicate MCMC-samples. **J**, Same as in **I** but for the Metaphase T0209.7 dataset. **K**, Same as in **I** but for the early Anaphase T0186.3.1 dataset. **L**, Same as in **I** but for the mid Anaphase T0234.6 dataset. **M, N, O, P** Comparison of experimentally determined length distribution of microtubules (dots) to the prediction of the highest likelihood model (solid line) for Metaphase T0186.1.1 (**M**), Metaphase T0209.7 (**N**), early Anaphase T0186.3.1 (**O**) and mid Anaphase T0234.6 (**P**).

References

Albertson, D. G., & Thomson, J. N. (1993). Segregation of holocentric chromosomes at meiosis in the nematode, Caenorhabditis elegans. *Chromosome Research*, *1*(1), 15-26.

Bakhoum SF, Genovese G, Compton DA. Deviant kinetochore microtubule dynamics underlie chromosomal instability. Curr Biol. 2009 Dec 1;19(22):1937-42. doi: 10.1016/j.cub.2009.09.055. Epub 2009 Oct 29.

Brenner, S. (1974). The genetics of Caenorhabditis elegans. *Genetics*, *77*(1), 71-94.

Brinkley BR, Cartwright J Jr (1975) Cold-labile and cold-stable microtubules in the mitotic spindle of mammalian cells. Ann N Y Acad Sci 253:428–439

Brugués, J., Nuzzo, V., Mazur, E., & Needleman, D. J. (2012). Nucleation and transport organize microtubules in metaphase spindles. *Cell*, *149*(3), 554-564.

Burbank KS, Groen AC, Perlman ZE, Fisher DS, Mitchison TJ. (2006). A new method reveals microtubule minus ends throughout the meiotic spindle. J Cell Biol. 6;175(3):369-75.

Connolly, A. A., Osterberg, V., Christensen, S., Price, M., Lu, C., Chicas-Cruz, K., ... & Bowerman, B. (2014). Caenorhabditis elegans oocyte meiotic spindle pole assembly requires microtubule severing and the calponin homology domain protein ASPM-1. *Molecular biology of the cell*, *25*(8), 1298-1311.

Dumont, J., Oegema, K., & Desai, A. (2010). A kinetochore-independent mechanism drives anaphase chromosome separation during acentrosomal meiosis. *Nature cell biology*, *12*(9), 894-901.

Edgar, L. G. (1995). Blastomere culture and analysis. In *Methods in cell biology* (Vol. 48, pp. 303-321). Academic Press.

Fabig, G., Kiewisz, R., Lindow, N., Powers, J. A., Cota, V., Mateo, L. J., ... & Müller-Reichert, T. (2020). eLife 2020;9:e50988 DOI: 10.7554/eLife.50988

Foreman-Mackey, D., Hogg, D. W., Lang, D., & Goodman, J. (2013). emcee: the MCMC hammer. *Publications of the Astronomical Society of the Pacific*, *125*(925), 306.

Geisterfer, Z. M., Zhu, D. Y., Mitchison, T., Oakey, J., & Gatlin, J. C. (2019). Microtubule growth rates are sensitive to global and local changes in microtubule plus-end density. *bioRxiv*, 849190.

Gilbert, P. F. C. (1972). The reconstruction of three-dimensional structure from projections and its application to electron microscopy II. Direct methods. *Proceedings of the Royal Society of London. Series B. Biological Sciences*, *182*(1066), 89-102.

Hassold, T., & Hunt, P. (2001). To err (meiotically) is human: the genesis of human aneuploidy. *Nature Reviews Genetics*, *2*(4), 280-291.

Holubcová, Z., Blayney, M., Elder, K., & Schuh, M. (2015). Error-prone chromosome-mediated spindle assembly favors chromosome segregation defects in human oocytes. *Science*, *348*(6239), 1143-1147.

Joly, N., Martino, L., Gigant, E., Dumont, J., & Pintard, L. (2016). Microtubule-severing activity of the AAA+ ATPase Katanin is essential for female meiotic spindle assembly. *Development*, *143*(19), 3604-3614.

Kremer, J. R., Mastronarde, D. N., & McIntosh, J. R. (1996). Computer visualization of three-dimensional image data using IMOD. *Journal of structural biology*, *116*(1), 71-76.

Kuo, Y. W., Trottier, O., Mahamdeh, M., & Howard, J. (2020). Effects of Severing Enzymes on the Length Distribution and Total Mass of Microtubules. *Biophysical Journal*, *118*(3), 598a.

Laband, K., Le Borgne, R., Edwards, F., Stefanutti, M., Canman, J. C., Verbavatz, J. M., & Dumont, J. (2017). Chromosome segregation occurs by microtubule pushing in oocytes. *Nature communications*, *8*(1), 1-11.

Labbé, J. C., McCarthy, E. K., & Goldstein, B. (2004). The forces that position a mitotic spindle asymmetrically are tethered until after the time of spindle assembly. *The Journal of cell biology*, *167*(2), 245-256.

MacKay, D. J., & Mac Kay, D. J. (2003). *Information theory, inference and learning algorithms*. Cambridge university press.

Mains PE, Kemphues KJ, Sprunger SA, Sulston IA, Wood WB. (1990). Mutations affecting the meiotic and mitotic divisions of the early Caenorhabditis elegans embryo. Genetics. 1990 Nov;126(3):593-605.

Mastronarde, D. N. (1997). Dual-axis tomography: an approach with alignment methods that preserve resolution. *Journal of structural biology*, *120*(3), 343-352.

McNally, K., Audhya, A., Oegema, K., & McNally, F. J. (2006). Katanin controls mitotic and meiotic spindle length. *The Journal of cell biology*, *175*(6), 881-891.

McNally, K. P., & McNally, F. J. (2011). The spindle assembly function of Caenorhabditis elegans katanin does not require microtubule-severing activity. *Molecular biology of the cell*, *22*(9), 1550-1560.

McNally, K., Berg, E., Cortes, D. B., Hernandez, V., Mains, P. E., & McNally, F. J. (2014). Katanin maintains meiotic metaphase chromosome alignment and spindle structure in vivo and has multiple effects on microtubules in vitro. *Molecular biology of the cell*, *25*(7), 1037-1049.

McNally, K. P., Panzica, M. T., Kim, T., Cortes, D. B., & McNally, F. J. (2016). A novel chromosome segregation mechanism during female meiosis. *Molecular biology of the cell*, *27*(16), 2576-2589.

Mullen, T. J., & Wignall, S. M. (2017). Interplay between microtubule bundling and sorting factors ensures acentriolar spindle stability during C. elegans oocyte meiosis. *PLoS genetics*, *13*(9), e1006986.

Needleman, D. J., Groen, A., Ohi, R., Maresca, T., Mirny, L., & Mitchison, T. (2010). Fast microtubule dynamics in meiotic spindles measured by single molecule imaging: evidence that the spindle environment does not stabilize microtubules. *Molecular biology of the cell*, *21*(2), 323-333.

O'Rourke SM, Carter C, Carter L, Christensen SN, Jones MP, Nash B, Price MH, Turnbull DW, Garner AR, Hamill DR, Osterberg VR, Lyczak R, Madison EE, Nguyen MH, Sandberg NA, Sedghi N, Willis JH, Yochem J, Johnson EA, Bowerman B.(2011). A survey of new temperature-sensitive, embryonic-lethal mutations in C. elegans: 24 alleles of thirteen genes. PLoS One. 2011 Mar 1;6(3):e16644.

Pelletier, L., O'Toole, E., Schwager, A., Hyman, A. A., & Müller-Reichert, T. (2006). Centriole assembly in Caenorhabditis elegans. *Nature*, *444*(7119), 619-623.

Redemann, S., Weber, B., Möller, M., Verbavatz, J. M., Hyman, A. A., Baum, D., ... & Müller-Reichert, T. (2014). The segmentation of microtubules in electron tomograms using Amira. In *Mitosis* (pp. 261-278). Humana Press, New York, NY.

Redemann, S., Baumgart, J., Lindow, N., Shelley, M., Nazockdast, E., Kratz, A., ... & Müller-Reichert, T. (2017). C. elegans chromosomes connect to centrosomes by anchoring into the spindle network. *Nature communications*, *8*(1), 1-13.

Redemann, S., Lantzsch, I., Lindow, N., Prohaska, S., Srayko, M., & Müller-Reichert, T. (2018). A switch in microtubule orientation during C. elegans meiosis. *Current Biology*, *28*(18), 2991-2997.

Rieder CL (1981) The structure of the cold-stable kinetochore fiber in metaphase PtK1 cells. Chromosoma 84(1):145–158

Schaedel, L., John, K., Gaillard, J., Nachury, M. V., Blanchoin, L., & Théry, M. (2015). Microtubules self-repair in response to mechanical stress. *Nature materials*, *14*(11), 1156-1163.

Schaedel, L., Triclin, S., Chrétien, D., Abrieu, A., Aumeier, C., Gaillard, J., ... & John, K. (2019). Lattice defects induce microtubule self-renewal. *Nature physics*, *15*(8), 830-838.

Schuh, M., & Ellenberg, J. (2007). Self-organization of MTOCs replaces centrosome function during acentrosomal spindle assembly in live mouse oocytes. *Cell*, *130*(3), 484-498.

Stalling, D., Westerhoff, M., & Hege, H. C. (2005). Amira: A highly interactive system for visual data analysis. *The visualization handbook*, *38*, 749-67.

Srayko, M., Kaya, A., Stamford, J., & Hyman, A. A. (2005). Identification and characterization of factors required for microtubule growth and nucleation in the early C. elegans embryo. *Developmental cell*, *9*(2), 223-236.

Srayko, M., O'Toole, E. T., Hyman, A. A., & Müller-Reichert, T. (2006). Katanin disrupts the microtubule lattice and increases polymer number in C. elegans meiosis. *Current biology*, *16*(19), 1944-1949.

Vemu, A., Szczesna, E., Zehr, E. A., Spector, J. O., Grigorieff, N., Deaconescu, A. M., & Roll-Mecak, A. (2018). Severing enzymes amplify microtubule arrays through lattice GTP-tubulin incorporation. *Science*, *361*(6404), eaau1504.

Walczak, C. E., Zong, H., Jain, S., & Stout, J. R. (2016). Spatial regulation of astral microtubule dynamics by Kif18B in PtK cells. *Molecular biology of the cell*, *27*(20), 3021-3030.

Weber, B., Greenan, G., Prohaska, S., Baum, D., Hege, H. C., Müller-Reichert, T., ... & Verbavatz, J. M. (2012). Automated tracing of microtubules in electron tomograms of plastic embedded samples of Caenorhabditis elegans embryos. *Journal of structural biology*, *178*(2), 129-138.

Weber, B., Tranfield, E. M., Höög, J. L., Baum, D., Antony, C., Hyman, T., ... & Prohaska, S. (2014). Automated stitching of microtubule centerlines across serial electron tomograms. *PloS one*, *9*(12).

Woog, I., White, S., Büchner, M., Srayko, M., & Müller-Reichert, T. (2012). Correlative light and electron microscopy of intermediate stages of meiotic spindle assembly in the early Caenorhabditis elegans embryo. In *Methods in cell biology* (Vol. 111, pp. 223-234). Academic Press.

Yang G, Houghtaling BR, Gaetz J, Liu JZ, Danuser G, Kapoor TM. (2007) Architectural dynamics of the meiotic spindle revealed by single-fluorophore imaging. Nat Cell Biol. 2007 Nov;9(11):1233-42.

Yu, C. H., Redemann, S., Wu, H. Y., Kiewisz, R., Yoo, T. Y., Conway, W., ... & Needleman, D. (2019). Central-spindle microtubules are strongly coupled to chromosomes during both anaphase A and anaphase B. *Molecular biology of the cell*, *30*(19), 2503-2514.